The 6dF Galaxy Survey: Samples, Observational Techniques and the First Data Release

D. Heath Jones, Will Saunders, Matthew Colless, Mike A. Read, Quentin A. Parker, Fred G. Watson, Lachlan A. Campbell, Daniel Burkey, Thomas Mauch, Malcolm Hartley, et al.

Mon. Not. R. Astron. Soc. **355,** 747–763 (2004) doi:10.1111/j.1365-2966.2004.08353.x

The 6dF Galaxy Survey: samples, observational techniques and the first data release

D. Heath Jones,[1⋆] Will Saunders,[2⋆] Matthew Colless,[2⋆] Mike A. Read,[3] Quentin A. Parker,[4,2] Fred G. Watson,[2⋆] Lachlan A. Campbell,[1⋆] Daniel Burkey,[3] Thomas Mauch,[5] Lesa Moore,[4] Malcolm Hartley,[2] Paul Cass,[2] Dionne James,[2] Ken Russell,[2] Kristin Fiegert,[2] John Dawe,[2] John Huchra,[6] Tom Jarrett,[7] Ofer Lahav,[8] John Lucey,[9] Gary A. Mamon,[10,11] Dominique Proust,[11] Elaine M. Sadler[5] and Ken-ichi Wakamatsu[12]

[1]*Research School of Astronomy & Astrophysics, The Australian National University, Weston Creek, ACT 2611, Australia*
[2]*Anglo-Australian Observatory, PO Box 296, Epping, NSW 2121, Australia*
[3]*Institute for Astronomy, Royal Observatory, Blackford Hill, Edinburgh EH9 3HJ*
[4]*Department of Physics, Macquarie University, Sydney 2109, Australia*
[5]*School of Physics, University of Sydney, NSW 2006, Australia*
[6]*Harvard-Smithsonian Centre for Astrophysics, 60 Garden St MS20, Cambridge, MA 02138-1516, USA*
[7]*Infrared Processing and Analysis Centre, California Institute of Technology, Mail Code 100-22, Pasadena, CA 91125, USA*
[8]*Department of Physics and Astronomy, University College London, Gower St, London WC1E 6BT*
[9]*Department of Physics, University of Durham, South Road, Durham DH1 3LE*
[10]*Institut d'Astrophysique de Paris (CNRS UMR 7095), 98 bis Bd Arago, F-75014 Paris, France*
[11]*GEPI (CNRS UMR 8111), Observatoire de Paris, F-92195 Meudon, France*
[12]*Faculty of Engineering, Gifu University, Gifu 501–1192, Japan*

Accepted 2004 August 23. Received 2004 August 13; in original form 2004 March 23

ABSTRACT

The 6dF Galaxy Survey (6dFGS) aims to measure the redshifts of around 150 000 galaxies, and the peculiar velocities of a 15 000-member subsample, over almost the entire southern sky. When complete, it will be the largest redshift survey of the nearby Universe, reaching out to about $z \sim 0.15$, and more than an order of magnitude larger than any peculiar velocity survey to date. The targets are all galaxies brighter than $K_{\rm tot} = 12.75$ in the 2MASS Extended Source Catalog (XSC), supplemented by 2MASS and SuperCOSMOS galaxies that complete the sample to limits of $(H, J, r_{\rm F}, b_{\rm J}) = (13.05, 13.75, 15.6, 16.75)$. Central to the survey is the Six-Degree Field (6dF) multifibre spectrograph, an instrument able to record 150 simultaneous spectra over the 5.°7-field of the UK Schmidt Telescope. An adaptive tiling algorithm has been employed to ensure around 95 per cent fibring completeness over the 17 046 deg^2 of the southern sky with $|b| > 10^\circ$. Spectra are obtained in two observations using separate V and R gratings, that together give $R \sim 1000$ over at least 4000–7500 Å and signal-to-noise ratio $\sim$10 per pixel. Redshift measurements are obtained semi-automatically, and are assigned a quality value based on visual inspection. The 6dFGS data base is available at http://www-wfau.roe.ac.uk/6dFGS/, with public data releases occurring after the completion of each third of the survey.

Key words: surveys – galaxies: clusters: general – galaxies: distances and redshifts – cosmology: observations – large-scale structure of Universe.

1 INTRODUCTION

Wide-scale redshift surveys such as the 2dF Galaxy Redshift Survey and Sloan Digital Sky Survey (2dFGRS, Colless et al. 2001b; SDSS, York et al. 2000) have made significant advances in our understanding of the matter and structure of the wider Universe. These include the precise determination of the luminosity function of galaxies (e.g. Folkes et al. 1999; Blanton et al. 2001; Cole et al. 2001; Cross et al. 2001; Madgwick et al. 2002; Norberg et al. 2002; Blanton et al. 2003), the space density of nearby rich galaxy clusters (De Propris et al. 2002; Goto et al. 2003), and large-scale structure formation and

⋆E-mail: heath@mso.anu.edu.au (DHJ); will@aao.gov.au (WS); colless@aao.gov.au (MC); fgw@aao.gov.au (FGW); lachlan@mso.anu.edu.au (LAC)

mass density (Peacock et al. 2001; Percival et al. 2001; Efstathiou et al. 2002; Lahav et al. 2002; Verde et al. 2002; Zehavi et al. 2002; Hawkins et al. 2003; Szalay et al. 2003).

While such surveys have also greatly refined our view of the local Universe, better determination of several key parameters can be made where a knowledge of galaxy mass can be combined with redshift. The 2dFGRS and SDSS surveys are both optically selected, inevitably biasing them in favour of currently star-forming galaxies. The 2dF and Sloan spectrographs also have fields of view too small to allow full sky coverage in realistic time-scales, limiting their utility for dynamical and cosmographic studies. The 6dF Galaxy Survey (6dFGS) is a dual redshift/peculiar velocity survey that endeavours to overcome the limitations of the 2dFGRS and SDSS surveys in these areas.

The primary sample for the 6dFGS is selected in the K_s band from the Two Micron All Sky Survey (2MASS) (Jarrett et al. 2000). The magnitudes used in the selection are estimated total magnitudes. These features combined mean that the primary sample is as unbiased a picture of the Universe, in terms of the old stellar content of galaxies, as is possible at the current time. The near-infrared (NIR) selection also enables the survey to probe closer to the Galactic equator before extinction becomes an issue; the survey covers the entire southern sky with $|b| > 10^{\circ}$.

The redshift of a galaxy includes both recessional and peculiar velocity components, so that a redshift survey alone does not furnish a true three-dimensional distribution for the galaxies. However, by measuring these components separately, it is possible to determine the three-dimensional distributions of both the galaxies and the underlying mass.

Observationally, significantly greater effort is required to obtain the distances and peculiar velocities of galaxies than their redshifts. Distance estimators based on the Fundamental Plane (FP) of early-type galaxies (Djorgovski & Davis 1987; Dressler et al. 1987), as used in the 6dFGS, require measurements of the internal velocity dispersions of the galaxies. Velocity dispersions demand a signal-to-noise ratio (S/N) in the spectrum at least 3–5 times higher than redshift measurements. Furthermore, the FP distance estimators need such spectroscopy to be supported by photometry which can be used to determine the surface-brightness profiles of the galaxies.

We measure peculiar velocities as the discrepancy between the redshift and the estimated distance. For realistic cosmologies, peculiar velocities increase weakly with distance, but remain $<1000\,\mathrm{km\,s^{-1}}$. Redshift errors are small, and have little or no dependence on distance. On the other hand, all existing distance estimators have significant, intrinsic and fractional, uncertainties in distance; for the FP estimators this uncertainty is typically about 20 per cent for a single galaxy measurement. This linear increase in the errors with distance, compared with more or less fixed peculiar velocities, means that the uncertainty on a single peculiar velocity becomes dominated by the intrinsic uncertainties at redshifts $cz \sim 5000\,\mathrm{km\,s^{-1}}$. Consequently, all previous peculiar velocity surveys have traced the velocity field, and hence the mass distribution, only out to distances of about $5000\,\mathrm{km\,s^{-1}}$ (for relatively dense field samples of individual galaxies; e.g. Dressler et al. 1987, Giovanelli et al. 1998; da Costa et al. 2000) or $15\,000\,\mathrm{km\,s^{-1}}$ (for relatively sparse cluster samples, where distances for multiple galaxies are combined; e.g. Lauer & Postman 1994; Hudson et al. 1999; Colless et al. 2001a). The smaller volumes are highly subject to cosmic variance, while the larger volumes are too sparsely sampled to reveal much information about the velocity field. In order to differentiate cosmological models, and constrain their parameters, both the survey volume and galaxy sampling need to be significantly increased. Moreover, since peculiar velocities amount to at most a few per cent of the velocity over much of the volume, both the underlying sample and the direct distance estimates have to be extraordinarily homogeneous, preferably involving unchanging telescopes, instrumental set-ups and procedures in each case.

The two facets of the 6dF Galaxy Survey are a redshift survey of 150 000 galaxies over the southern sky, and a peculiar velocity survey of a subset of some 15 000 of these galaxies.

The aims of the redshift survey are:

(i) To take a near-infrared selected sample of galaxies and determine their luminosity function as a function of environment and galaxy type. From these, the stellar mass function and mean stellar fraction of the local Universe can be ascertained and compared to the integrated stellar mass inferred from measures of cosmic star-formation history, extending the work of Cole et al. (2001), Kochanek et al. (2001) and Bell et al. (2003).

(ii) To measure galaxy clustering on both small and large scales and its relation to stellar mass. In doing so, the 6dFGS will provide new insight into the scale-dependence of galaxy biasing and the relationship between the integrated star-formation histories of galaxies and the large-scale structure of the dark matter.

(iii) To determine the power spectrum of this galaxy clustering on scales similar to those spanned by the 2dF Galaxy Redshift Survey and Sloan Digital Sky Surveys.

(iv) To delineate the distribution of galaxies in the nearby Universe. The 6dFGS will not cover as many galaxies as either the 2dF Galaxy Redshift Survey or Sloan Digital Sky Survey. However, because it is a large-volume survey of nearby galaxies, it provides the ideal sample on which to base a peculiar velocity survey. In this respect, the complete 6dFGS will be more than 10 times larger in number and cover twice the volume of the PSCz Survey (Saunders et al. 2000), previously the largest survey of the local Universe.

(v) To furnish a complete redshift catalogue for future studies in this regime. Precise distance measures impose stronger demands on signal-to-noise ratio than do redshifts. With such higher-quality spectra, it it is also possible to infer, by comparison with stellar population models, properties of the underlying stellar population such as ages and chemical abundances. Having such measurements along with the galaxy mass and knowledge of its local environment will afford unprecedented opportunities to understand the processes driving galaxy formation and evolution.

This redshift catalogue will provide the basis for a volume-limited sample of early-type galaxies for the peculiar velocity survey. The aims of the peculiar velocity survey are:

(i) A detailed mapping of the density and peculiar velocity fields to around $15\,000\,\mathrm{km\,s^{-1}}$ over half the local volume.

(ii) The inference of the ages, metallicities and star-formation histories of E/S0 galaxies from the most massive systems down to dwarf galaxies. The influence of local galaxy density on these parameters will also be of key interest to models of galaxy formation.

(iii) To understand the bias of galaxies (number density versus total mass density field) and its variation with galaxy parameters and environment.

One novel feature of the 6dF Galaxy Survey compared to earlier redshift and peculiar velocity surveys is its near-infrared source selection. The main target catalogues are selected from the Two Micron All Sky Survey (2MASS; Jarrett et al. 2000) using total galaxy magnitudes in *JHK*. There are several advantages of choosing galaxies in these bands. First, the near-infrared spectral energy distributions (SEDs) of galaxies are, in general, dominated by the

near-infrared light of their old stellar populations, which also provides the best photometric estimator of their stellar mass. Traditionally, surveys have selected target galaxies in the optical where galaxy SEDs are dominated by younger, bluer stars, and so are more indicative of the star-formation rate than the total stellar mass. Second, the E/S0 galaxies that will provide the best targets for Fundamental Plane peculiar velocity measures represent the largest fraction by galaxy type of near-infrared-selected samples. Finally, the effects of dust extinction are minimal at long wavelengths. In the target galaxies, this means that the total near-infrared luminosity is not dependent on galaxy orientation and so provides a reliable measure of galaxy mass. In our own Galaxy, it means the 6dFGS can map the local Universe nearer to the plane of the Milky Way than would be possible through optical selection.

In this paper we describe the key components contributing to the realization of the 6dF Galaxy Survey. Section 2 describes the Six-Degree Field instrument; Section 3 details the compilation of the input catalogues and the optimal placement of fields and fibres on sources therein; Section 4 outlines the methods used to obtain and reduce the spectra, and derive redshifts from them; Section 5 summarizes the First Data Release of 46 474 unique galaxy redshifts and describes the 6dF Galaxy Survey on-line data base; Section 6 provides concluding remarks.

2 THE SIX-DEGREE FIELD SPECTROGRAPH

Central to the 6dFGS is the Six-Degree Field multi-object fibre spectroscopy facility (hereafter referred to as 6dF), constructed by the Anglo-Australian Observatory (AAO) and operated on the United Kingdom Schmidt Telescope (UKST). This instrument has three major components: (1) an r–θ robotic fibre positioner; (2) two interchangeable 6dF field plates that contain the fibres to be positioned; and (3) a fast Schmidt spectrograph that accepts the fibre slit from a 6dF field plate. The process of 6dF operation involves configuring a 6dF field plate on target objects, mounting this configured plate at the focal surface of the UKST and feeding the output target fibre bundle into an off-telescope spectrograph. While one target field is being observed the other field plate can be configured.

6dF can obtain up to 150 simultaneous spectra across the $5\overset{\circ}{.}7$-diameter field of the UKST. Fuller descriptions of the 6dF instrument have been given elsewhere (Parker et al. 1998; Watson et al. 2000; Saunders et al. 2001); here we summarize only those features important to the Galaxy Survey.

The 6dF positioner, though building on the expertise and technology successfully developed and employed in the 2dF facility of AAO (e.g. Lewis et al. 2002), and in previous incarnations of fibre-fed spectrographs at the UKST such as FLAIR (Parker & Watson 1995), is nevertheless a significant departure in both concept and operation. 6dF employs an r–θ robotic fibre positioner constructed as a working prototype for the OzPoz fibre positioner built under contract by the AAO and now commissioned on the European Southern Observatory Very Large Telescope. This fibre-placement technology can place fibre buttons directly and accurately on to the convex focal surface of the UKST, via a curved radial arm matched to the focal surface. This is coupled with a complete $>360^\circ$ θ-travel and with a pneumatically controlled fibre gripper travelling in the z-direction. Gripper positioning is honed (to $<10\,\mu$m) using an in-built small CCD camera to permit centroid measurement from back-illuminated images of each fibre.

Unlike 2dF, the 6dF positioning robot is off-telescope, in a special enclosure on the dome floor. Two identical field plate units are available, which allows one to be mounted on the telescope taking observations whilst the other is being configured by the 6dF robot. Each field plate contains a ring of 154 fibre buttons comprising 150 science fibres and four bundles of guide fibres all arranged around the curved field plate. Each 100 μm ($6\overset{''}{.}7$) science fibre is terminated at the input end by a 5-mm diameter circular button, containing an elongated SF2 prism to deflect the light into the fibre and a strong rare-earth magnet for adhesion to the field plate. Targets closer than $5\overset{'}{.}7$ on the sky cannot be simultaneously configured due to the clearances required to avoid collisions and interference between buttons. The buttons and trailing fibres are incorporated into individual retractors housed within the main body of the field plate under slight elastic tension. The 150 target fibres feed into a fibre cable wrap 11-m long, and terminate in a fibre slit-block mounted in the 6dF spectrograph.

A full field configuration takes around 30–40 min depending on target disposition and target numbers, plus about half this time to park any prior configuration. This is less than the 1.5–2.5 h (depending on conditions) spent by a configured field plate in the telescope. There is, however, a 25–30 min overhead between fields, needed for parking the telescope, taking arcs and flats, manually unloading and loading the field plates, taking new arcs and flats, and acquiring the new field. The acquisition is via four guide fibres, each consisting of $7 \times 100\,\mu$ m fibres hexagonally packed to permit direct imaging from four guide stars across the field plate. The guide fibres proved extremely fragile in use, and also hard to repair until a partial redesign in 2002; as a result of this a significant fraction of the data was acquired with three, or occasionally even two, guide fibres, with consequent loss of acquisition accuracy and signal-to-noise ratio.

The spectrograph is essentially the previous bench-mounted FLAIR II instrument[1] but upgraded with new gratings, CCD detector and other refinements. The instrument uses a 1032×1056 pixel^2 Marconi CCD47-10 device, with 13-μm pixels.

All 6dFGS data taken prior to 2002 October used 600V and 316R reflection gratings, covering 4000–5600 Åand 5500–8400 Å, respectively. Subsequent data uses Volume-Phase transmissive Holographic (VPH) 580V and 425R gratings from Ralcon Development Laboratory, with improved efficiency, focus and data uniformity. The wavelength coverage is 3900–5600 Å and 5400–7500 Å and the grating and camera angles (and hence dimensionless resolutions) are identical. The peak system efficiency (good conditions and acquisition, wavelengths near blaze, good fibres) is 11 per cent, but can be much less.

The marginally lower dispersion of the 580V VPH grating, as compared with the 600V reflection grating, is compensated by the better focus allowed by the reduced pupil relief.

The UK Schmidt with 6dF is well-suited to low-to-medium resolution spectroscopy of bright ($V < 17$), sparsely distributed sources (1–50 deg^{-2}). It fills the gap left open by 2dF for large, shallow surveys covering a significant fraction of the total sky. In terms of the $A\,\Omega$ (telescope aperture $\times$ field of view) figure-of-merit, UKST/6dF is similar to AAT/2dF and Sloan.

3 SURVEY DESIGN

3.1 Overview

Surveys that cover the sky in a new waveband (such as 2MASS) are invariably shallow and wide-angle, as this maximizes the return (in terms of sample numbers), for the intrinsically difficult observations.

[1] Fibre-Linked Array-Image Reformatter, Parker & Watson (1995).

Table 1. Wide-area redshift surveys.

Survey	Magnitude limits	Area (sr)	Sample ($\times 10^3$)	Reference
Centre for Astrophysics Survey (CfA2)	$B(0) \leqslant 15.5$	2.09	4.391	Huchra et al. (1999)
Southern Sky Redshift Survey (SSRS)	$B(0) \leqslant 15.5$	1.70	5.369	da Costa et al. (1998)
Stromlo-APM Redshift Survey (SAPM)	$b_{\rm J} \leqslant 17.15$	1.31	1.769	Loveday et al. (1992)
Point-Source Catalog z-Survey (PSCz)	$S_{60} \leqslant 0.6$ Jy	10.6	15.411	Saunders et al. (2000)
2dF Galaxy Redshift Survey (2dFGRS)	$b_{\rm J} \leqslant 19.45$	0.61	221.414	Colless et al. (2001b)
Sloan Digital Sky Survey (SDSS)[a]	$r \leqslant 17.77$	2.20[b]	~ 630[b]	Glazebrook, priv. comm.
6dF Galaxy Survey (6dFGS)[a]	$(K, H, J, r_{\rm F}, b_{\rm J}) \leqslant (12.75, 13.05, 13.75, 15.6, 16.75)$	5.19	$\sim$150	This paper.

[a]Currently in progress.
[b]Estimated from the new SDSS target coverage of $\sim$7000 deg^2, revised from the original $\sim$10 000 deg^2 and $\sim$900 000 galaxies.

This also holds true for the *IRAS*, *ROSAT*, HIPASS, NVSS and SUMSS surveys. Other projects, such as finding peculiar velocities, are even more strongly driven to being as shallow and wide-angled as possible; and any project using galaxy distributions to predict dynamics requires just as great sky coverage as possible. All such surveys are hence uniquely matched to 6dF, with its ability to map the whole sky in realistic time-scales.

The scope of large-scale redshift surveys has increased substantially over the past two decades. The major redshift surveys listed in Table 1 have revealed the complex structure of the galaxy distribution over large volumes of the low-redshift Universe. At the same time, the quality of galaxy photometry over large areas of sky has improved from the early photographic magnitudes to scanned photographic plate photometry and then digital photometry. The latest generation of redshift surveys, including the 6dFGS, uses digital photometry of large areas of sky and purpose-built multiplexing spectrographs measuring hundreds or thousands of redshifts in a night.

Burkey & Taylor (2004) have recently studied how the scientific returns of 6dFGS should be optimized in light of existing large-scale data sets such as the 2dFGRS and SDSS. Their analysis shows that the combined redshift (z) and peculiar velocity (v) components of the 6dFGS give it the power to disentangle the degeneracy between several key parameters of structure formation, listed in Table 2. They demonstrate that $A_{\rm g}$, Γ and β can be determined to within around 3 per cent if only the redshift survey is used, although $\omega_{\rm b}$ and $r_{\rm g}$ are much less well-constrained. If the combined z and v data are used, all of $A_{\rm g}$, Γ, β and $r_{\rm g}$ can be determined to within 2–3 per cent. The change in β and $r_{\rm g}$ on different spatial scales can also be determined to within a few per cent. Clearly the advantage of the 6dFGS in understanding structure formation comes from its large-scale determination of galaxy masses, in addition to distances.

Burkey & Taylor also calculate the optimal observing strategy for 6dFGS, and confirm that the dense sampling and widest possible areal coverage are indeed close to optimal for parameter estimation.

Table 2. Cosmological parameters readily measurable from the 6dF Galaxy Survey.

	Parameter
b	bias parameter
$A_{\rm g} = bA_{\rm m}$	galaxy power spectrum amplitude
$A_{\rm v} = \Omega_{\rm m}^{0.6} A_{\rm m}$	velocity field amplitude
$\Gamma = \Omega_{\rm m} h$	power spectrum shape parameter
$\omega_{\rm b} = \Omega_{\rm b} h$	mass density in baryons
$\beta = \Omega_{\rm m}^{0.6}/b$	redshift-space distortion parameter
$r_{\rm g}$	luminous –dark matter correlation coefficient

3.2 Observational considerations

The original science drivers for the 6dF project were an all-southern-sky redshift survey of NIR-selected galaxies, and a large peculiar velocity survey of early-type galaxies. Three instrumental considerations led to the observations for these projects being merged. First, the combination of the physical size of the 6dF buttons (5 mm), the small plate scale of the Schmidt ($67\farcs14$ mm^{-1}), and the strong angular clustering of the shallow and mostly early-type input catalogues, meant that acceptable ($\sim$90 per cent) completeness could only be achieved by covering the sky at least twice, in the sense that the sum of the areas of all tiles observed be at least twice the actual area of sky covered. Secondly, the spectrograph optics and CCD dimensions did not simultaneously permit an acceptable resolution ($R \sim 1000$) over the required minimal wavelength range 4000–7500 Å, and this meant that each field had to be observed separately with two grating set-ups. Thirdly, the robot configuring times, and the overheads between fields (parking the telescope, changing field plates, taking calibration frames, acquiring a new field), meant that observations less than 1–2 h/field were not an efficient use of the telescope. Together, these factors meant that the redshift survey would necessarily take longer than originally envisaged. However, careful consideration of the effects of signal-to-noise ratio and resolution on velocity width measurements (see Wegner et al. 1999) led us to conclude that for the luminous, high-surface-brightness galaxies expected to dominate the peculiar velocity survey, the resolution and signal-to-noise ratio expected from the redshift survey observations (in some case repeated to increase S/N) would in general allow velocity widths to be determined to the required accuracy. Therefore, in early 2001 a decision was made to merge the observations for the two surveys.

These observational considerations implied that the survey would be of $\sim$1500 fields, with $\sim$1 hour integration time per field per grating, and covering 4000–7500 Å. With 100–135 fibres available for targets per field, this meant 150 000–200 000 observations could be made in total. Given the $\sim$100 000 targets desired for the primary K-selected survey, and an expected 20 per cent contingency for re-observation (either because of failures or to increase S/N), there remained the opportunity to include other samples in the survey, especially if they required lower levels of observational completeness than the primary sample. Some of these were selected by the Science Advisory Group to fill out the sample to provide substantial flux-selected samples at H, J, I, $b_{\rm J}$, and $r_{\rm F}$ wavebands; others were invited from the community as an announcement of opportunity, and resulted in a wide variety of X-ray, radio, optical, near- and far-infrared selected extragalactic samples being included. It is striking that most of these additional samples derive from the first sky surveys in a new waveband, and also that most of them could not

be undertaken on any other telescope, being too large for long-slit work, but too sparse for multiplexing in their own right.

3.3 The primary sample

The primary redshift (z-survey) sample is a magnitude-limited selection drawn from the 2MASS Extended Source Catalog, version 3 (2MASS XSC; Jarrett et al. 2000). Since the survey is attempting a 'census' of the local Universe, we want to avoid any bias against lower-surface-brightness galaxies, and ideally we would use total magnitudes. 2MASS data *do* include total magnitudes, estimated from curves of growth, and these are reliable for high galactic latitudes and/or very bright galaxies. For galaxies at lower latitude, 2MASS does not have the depth nor resolution to derive robust total magnitudes to our desired flux limit. On the other hand, 2MASS includes very robust isophotal magnitudes ($K_{\rm iso}$) and diameters to an elliptical isophote of $\mu_K = 20\,{\rm mag\,arcsec^{-2}}$. We found that we were able to make a simple surface-brightness correction to these standard isophotal magnitudes, which gave an excellent approximation to the total magnitudes, where they were reliably determined for high-latitude galaxies (Fig. 1):

$$K_{\rm tot} = K_{\rm iso} - 1.5 \exp\left[1.25 \times (\overline{\mu_{K20}} - 20)\right]. \quad (1)$$

Here, $\overline{\mu_{K20}}$ is the mean surface brightness within the $\mu_K = 20$ elliptical isophote, and with a maximum allowed correction of 0.5 mag. This 'corrected' isophotal magnitude was also extremely robust to stellar contamination. There remains a smaller second-order bias dependent on the convexity of the profile. Further details are in Burkey (2004). In all bands, galaxy selection has been made using magnitudes uncorrected for Galactic extinction.

A latitude cut of $|b| \geqslant 10^\circ$ was imposed, mostly because extinctions closer to the plane would demand much greater integration times. The sample was limited to the southern hemisphere ($\delta < 0^\circ$).

Our final selection was then 113 988 galaxies with $K_{\rm tot} < 12.75$, corresponding approximately to $K_{20} < 13$ mag for typical K-selected galaxies.

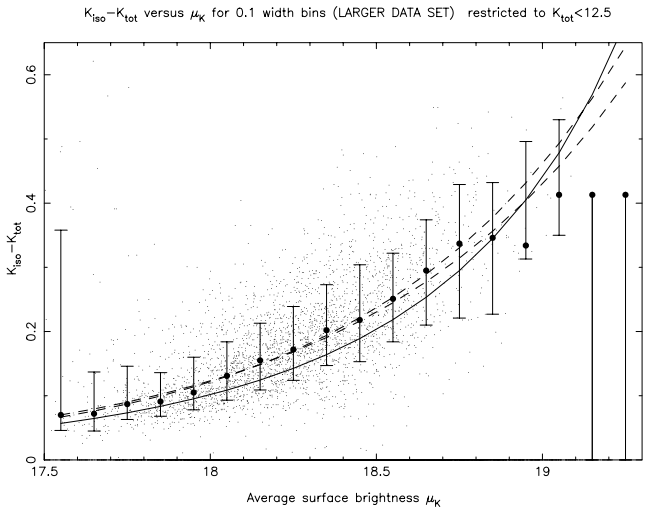

Figure 1. Correlation between isophotal –total magnitude deficit and surface brightness, versus a simple exponential disc model (solid curve) and the finally adopted correction (upper dashed curve). Isophotal magnitudes are measured to an isophote of $\mu_K = 20\,{\rm mag\,arcsec^{-2}}$. There is increasing Malmquist bias at lower surface brightnesses, since galaxies with large deficits are increasingly unlikely to enter the 2MASS catalogue.

3.4 The additional samples

Thirteen other smaller extragalactic samples are merged with the primary sample. These include secondary 2MASS selections down to $H_{\rm tot} = 13.05$ and $J_{\rm tot} = 13.75$ over the same area of sky, constituting an additional ∼5000 sources. Optically selected sources from the SuperCOSMOS catalogue (Hambly et al. 2001) with $r_{\rm F} = 15.6$ and $b_J = 16.75$, $|b| > 20^\circ$, were included, constituting a further ∼20 000 galaxies. The remaining miscellaneous piggy-back surveys contribute a further ∼29 000 galaxies in various regions of the sky. These samples heavily overlap, greatly increasing the efficiency of the survey – the combined grand sum of all the samples amounts to 500 000 sources, but these represent only 174 442 different sources when overlap is taken into account. However, at the current rate of completion, we estimate that the eventual number of 6dF galaxy redshifts will be around 150 000.

Table 3 summarizes the breakdown of source catalogues contributing to the master target list. Also shown is the relative weighting given to each sample in the field allocation process, and the maximum coverage expected for each survey given that field allocation. In total there are 167 133 objects with field allocations of which two-thirds are represented by the near-infrared-selected sample. A further 7309 unallocated sources brings the total target list to 174 442. The mean surface density of this primary sample is $7\,{\rm deg^{-2}}$. Literature redshifts have been incorporated into the redshift catalogue, 19 570 of these from ZCAT (Huchra et al. 1999) and 8444 from the 2000 deg^2 in common with the 2dF Galaxy Redshift Survey (Colless et al. 2001b). For the primary sample, all galaxies are observed, even where the redshift is already known, to give a complete spectroscopic sample at reasonable resolution ($R \sim 1000$) and signal-to-noise ratio (S/N $\sim 10\,{\rm pixel^{-1}}$). Both tiling (Section 3.3) and configuring (3.4) of targets within individual fields used the weights to assign priorities.

3.5 Peculiar velocity survey

Peculiar velocities are a vital probe of the large-scale mass distribution in the local Universe that does not depend on the assumption that light traces mass. Early work (Lynden-Bell et al. 1988) made the unexpected discovery of a large ($\sim$600 km s^{-1}) outflow (positive peculiar velocities) in the Centaurus region. This led to the idea of a large extended mass distribution, nicknamed the Great Attractor (GA), dominating the dynamics of the local Universe. Lynden-Bell et al. estimated this structure was located at (l, b, cz) $\sim$ (307°, 7°, $4350 \pm 350\,{\rm km\,s^{-1}}$) and had a mass of $\sim 5 \times 10^{16}\,{\rm M_\odot}$. Attempts to measure the expected GA backside infall have proved controversial and some workers have argued for a continuing high-amplitude flow beyond the GA distance perhaps resulting from a more distant gravitational pull of the Shapley concentration (312°, 31°, 14 000 km s^{-1}) (Scaramella et al. 1989; Hudson et al. 1999).

The goal of the peculiar velocity (v-survey) is to measure peculiar velocities for an all-southern-sky sample of galaxies. In principle, we can extend the redshift field to the northern hemisphere by including PSCz and other northern z-surveys (e.g. Branchini et al. 1999; Huchra et al. 1999). Peculiar velocities are measured for early-type galaxies through the Fundamental Plane parameters from 2MASS images and 6dF spectroscopy to give velocity dispersions. The v-survey sample consists of all early-type galaxies from the primary z-survey sample that are sufficiently bright to yield precise velocity dispersions. Because we cover the sky twice, suitable candidate galaxies (selected on the basis of either 2MASS morphology or first-pass 6dF spectroscopy) can be observed a second time in

Table 3. The 6dFGS target samples used to define the tiling. There are also samples of 6843 SUMSS sources (Sadler, Sydney) and 466 Durham/UKST Galaxy Survey sources (Shanks, Durham), not used in the tiling but included for serendipitious observation. Surveys with higher-priority indices carry greater importance in the allocation of fields. 'Coverage' is as expected from the tiling simulations; in practice fibre breakages and imperfect fibre assignment reduce these numbers, especially for lower-priority samples.

Sample (Contact, Institution)	Weight	Total	Coverage
2MASS $K < 12.75$ (Jarret, IPAC)	8	113988	94.1 per cent
2MASS $H < 13.05$ (Jarret, IPAC)	6	3282	91.8 per cent
2MASS $J < 13.75$ (Jarret, IPAC)	6	2008	92.7 per cent
SuperCOSMOS $r_F < 15.6$ (Read, ROE)	6	9199	94.9 per cent
SuperCOSMOS $b_J < 16.75$ (Read, ROE)	6	9749	93.8 per cent
Shapley (Proust, Paris-Meudon)	6	939	85.7 per cent
ROSAT All-Sky Survey (Croom, AAO)	6	2913	91.7 per cent
HIPASS ($>4\,\sigma$) (Drinkwater, Queensland)	6	821	85.5 per cent
IRAS FSC $6\,\sigma$ (Saunders, AAO)	6	10707	94.9 per cent
DENIS $J < 14.00$ (Mamon, IAP)	5	1505	93.2 per cent
DENIS $I < 14.85$ (Mamon, IAP)	5	2017	61.7 per cent
2MASS AGN (Nelson, IPAC)	4	2132	91.7 per cent
Hamburg-ESO Survey (Witowski,Potsdam)	4	3539	90.6 per cent
NRAO-VLA Sky Survey (Gregg, UCDavis)	4	4334	87.6 per cent
Total		167133	93.3 per cent

order to extend the v-survey sample to fainter limits. Based on the high fraction of early-type galaxies in the K-selected sample and the signal-to-noise ratio obtained in our first-pass spectroscopy, we expect to measure distances and peculiar velocities for 15 000 galaxies with $cz < 15\,000\,\mathrm{km\,s^{-1}}$.

When linked with the *predicted* peculiar velocities from all-sky redshift surveys like the PSCz (Branchini et al. 1999), a value for Ω can be found that is independent of cosmic microwave background measurements.

3.6 Field placement and tiling algorithm

The survey area is 17 046 deg^2, meaning that the 1360 6dF fields (5.°7-diameter) contain a mean of 124 sources per field and cover the sky twice over. An adaptive tiling algorithm was employed to distribute the fields ('tiles') across the sky to maximize uniformity and completeness, described in full in Campbell et al. (2004). In brief, this consisted of a merit function, which was the priority-weighted sum ($P = \beta^p$, Section 3.3) of allocated targets; a method for rapidly determining fibring conflicts between targets; a method of rapidly allocating targets to a given set of tiles so as to maximize the merit function; and a method to make large or small perturbations to the tiling. Tiles were initially allocated in random target positions, and the merit function maximized via the Metropolis algorithm (Metropolis et al. 1953).

It quickly became clear that the clusters were too 'greedy' under this scheme, in the sense that the completeness was higher in these regions. This is easily seen by considering a tiling with a uniform level of incompleteness everywhere, but with one last tile still to be placed: this will always go to the densest region, as there is the largest density of unconfigured targets here also. To counter this effect, we inversely weighted each galaxy by the local galaxy surface density (as determined from the primary sample) on tile-sized scales; in the above example this means the final tile can be placed anywhere with equal merit. This achieved our aim of consistent completeness, at a very small penalty in overall completeness. It broke down in the heart of the Shapley supercluster, with galaxy densities orders of magnitude higher than elsewhere, and we added 10 tiles by hand in this region.

Two major tiling runs of the 6dFGS catalogue have been done: the first in 2002 April before commencement of observations (*version A*), and a second revised tiling in 2003 February after the first year of data (*version D*). The revision was due to the higher-than-expected rate at which fibres were broken and temporarily lost from service (Fig. 2), and a major revision in the primary sample itself from IPAC.

Fig. 3 shows the relationships between the full source list (*top*), those that remained unobserved at the time of the *version D* tiling

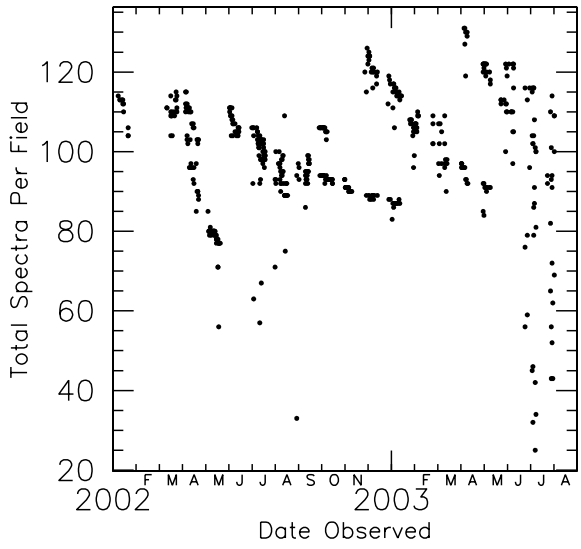

Figure 2. Total number of spectra obtained per field between 2002 January and 2003 June. The upper envelope shows the maximum number of fibres available at any one time. It tracks the loss of fibres over time, and how field plate #1 was taken out of service for 2003 January–February for a major fibre repair. The large scatter seen from the end of 2003 June is due to a change in observing strategy, from field choice maximizing fibre allocation to one aimed at completing areas of sky.

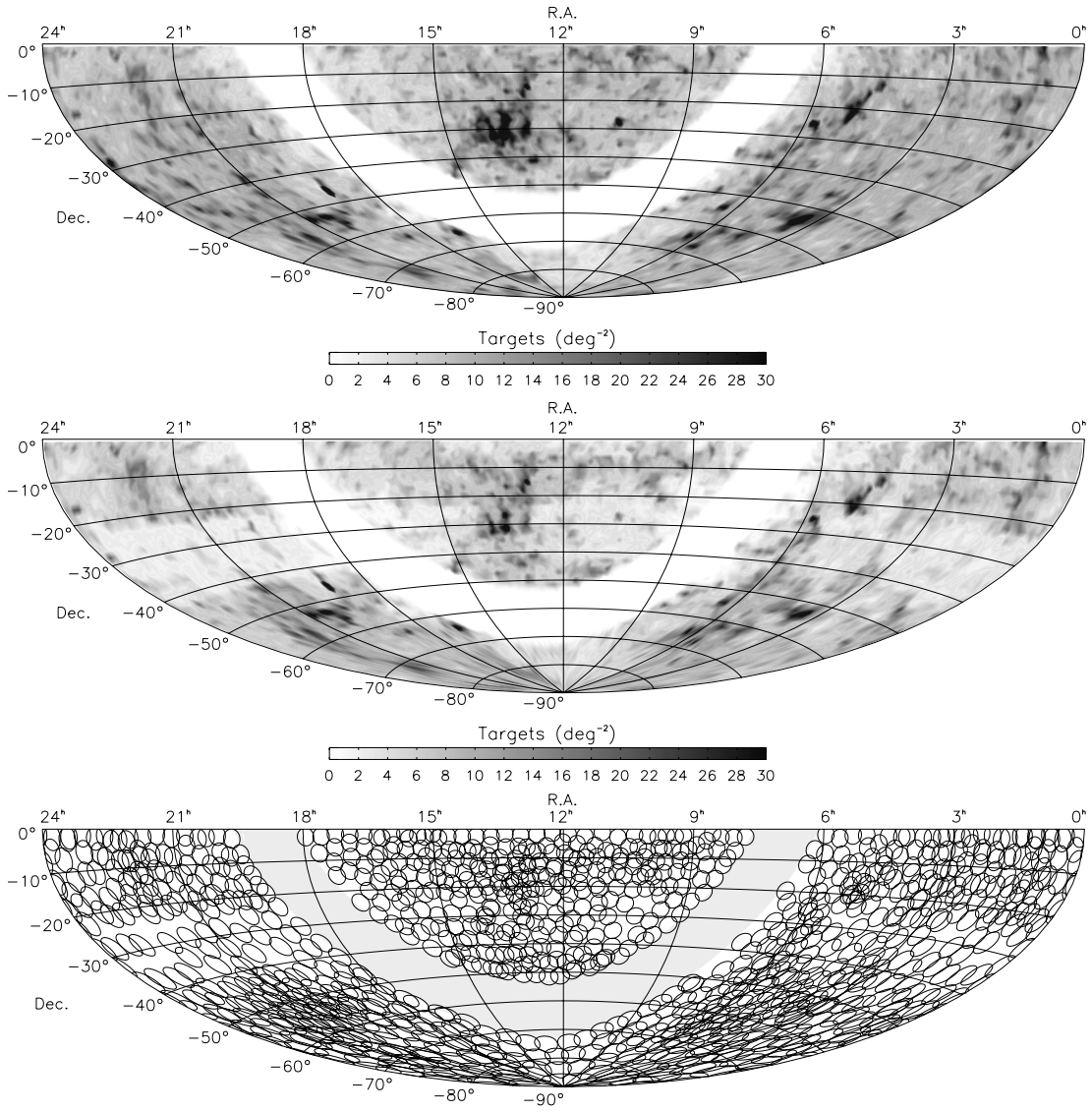

Figure 3. (Top) Sky distribution of all targets in the source catalogues. (Middle) Distribution of unobserved sources at the time of the version D tiling allocation in 2003 February. Note how most of the fields observed between the versions A and D were confined to the central strip (-23° to -42° declination). (Bottom) Optimal distribution of tiles based on the unobserved sources at the time of version D.

allocation (*middle*), and the optimal tile placement to cover these (*bottom*).

Tests of the two-point correlation function were made on the sample selected through the final tiling allocation, to see what systematic effects might arise from its implementation. Mock catalogues were generated, with correlation function as observed by the 2dF Galaxy Redshift Survey (Hawkins et al. 2003), these were tiled as the real data and the resulting two-point correlation function determined and compared with the original. This revealed an undersampling on scales up to $\sim 1\ h\,\mathrm{Mpc}^{-1}$, clearly the result of the fibre-button proximity limit. No bias was seen on larger scales.

Theoretical tiling completenesses of around 95 per cent were achievable for all except the lowest priority samples, and variations in uniformity were confined to <5 per cent. However, fibre breakages have meant that 6dFGS has consistently run with many fewer fibres than anticipated, impacting on the completeness of the lower priority samples in particular. With a fixed time-line for the survey (mid-2005) and a fixed number of fields to observe, there is little choice in the matter.

3.7 Fibre assignment

Within each tile, targets are assigned to fibres by the same CONFIGURE software used by the 2dF Galaxy Redshift Survey. This iteratively tries to find the largest number of targets assigned to fibres, and the highest-priority targets. Early configurations (until mid-2003) were usually tweaked by hand to improve target yield; after that date a revised version of CONFIGURE was installed with much improved yields and little or no further tweaking was in general made.

4 SURVEY IMPLEMENTATION

4.1 Observational technique

Field acquisition with 6dF is carried out using conventional guide-fibre bundles. Four fibre buttons are fitted with coherent bundles of seven fibres rather than a single science fibre. Fibre diameter is 100 μm (6.″7) and the guide fibres are in contact at the outer cladding to

give a compact configuration ∼20 arcsec in diameter. These fibres are 5-m long and feed the intensified CCD acquisition camera of the telescope. The use of acquisition fibres of the same diameter as the science fibres is suboptimal, but in practice the four guide-fibre bundles give good alignment, particularly as guide stars near the edge of the field are always chosen.

Guide stars are selected from the Tycho-2 catalogue (Hoeg et al. 2000), and have magnitudes typically in the range $8 < V < 11$. Field acquisition is straightforward in practice, and the distortion modelling of the focal surface of the telescope is sufficiently good that a field rotation adjustment is not usually required, other than a small standard offset.

Each field is observed with both V and R gratings that are later spliced to reconstruct a single spectrum from these two observations. Integrations are a minimum of 1 h for the V spectrum and 0.5 h for the R spectrum, although these times are increased in poor observing conditions. This gives spectra with typical S/N around 5–10 pixel^{-1}, yielding about 90 per cent redshift completeness.

This observing strategy typically allows 3–5 survey fields to be observed on a clear night, depending on season. With 75 per cent of the available dark and grey time on the UKST assigned to 6dFGS (amounting to 175 nights per year), and an average clear fraction of 60 per cent, we typically observe about 400 fields per year. The observational strategy is to divide the sky into three declination strips. Initially, the survey has concentrated on the $\delta = -30^\circ$ declination strip (actually $-42^\circ < \delta < -23^\circ$). The equatorial strip ($-23^\circ < \delta < 0^\circ$) will be done next, and then finally the polar cap ($\delta < -42^\circ$).

Observations started in 2001 June, though final input catalogues and viable reduction tools were not available until 2002. Early data suffered from various problems, including poorer spectrograph focus due to misalignment within the camera; poorer quality control; and use of preliminary versions of the 2MASS data, leading to many observed sources being dropped from the final sample. The 2001 data are not included in this data release.

Initial observations were carried out at mid-latitudes for observational convenience, with the actual band corresponding to one of the Additional Target samples. Excursions from this band were made to target other Additional Target areas, where separate telescope time had been allotted to such a programme, but the observations could be fruitfully folded in to 6dFGS.

The observing sequence conventionally begins with R data (to allow a start to be made in evening twilight). With the telescope at access park position, a full-aperture flat-field screen is illuminated with calibration lamps. First of these is a set of quartz lamps to give a continuum in each fibre. This serves two purposes: (a) the loci of the 150 spectra are defined on the CCD, and (b) the differences between the extracted spectra of the smooth blackbody lamp allow flat-fielding of the signatures introduced into the object spectra by pixel-to-pixel variations and fibre –fibre chromatic throughput variations. Then the wavelength-calibration lamps are exposed, HgCd + Ne for the R data and HgCd + He for the V data. After the R calibration exposure, the field is acquired and the 3 × 10-min red frames obtained. Once they are completed, the grating is changed remotely from the control room and the 3 × 20-min V frames obtained. At the end of the sequence, the V wavelength calibration and flat-field exposures are made.

With the change of field comes a change of slit-unit (because of the two 6dF field plates), so all the calibrations must be repeated for the next field. Usually, the reverse waveband sequence is followed, i.e. beginning with V and ending with R. This process continues throughout the night, as conditions allow.

4.2 Reduction of spectra

The reduction of the spectra uses a modified version of the 2DFDR package developed for the 2dF Galaxy Redshift Survey. Unlike 2dF data, tramline fitting is done completely automatically, using the known gaps in the fibres to identify uniquely the spectra with their fibre number. Because of computing limitations, TRAM rather than FIT extractions are performed. FIT extractions would reduce cross-talk between fibres, but this is already small for 6dF compared with 2dF. Scattered light subtraction is not in general performed, unless there is specific reason for concern, such as during periodic oil-contamination episodes within the dewar. Again, scattered light performance is better with 6dF in general than with 2dF.

The extracted spectra for each field are combined, usually weighted by S/N to cope with variable conditions. The S/N is computed at this stage, and a S/N per pixel of 10 in each of the V and R frames usually indicates a satisfactorily observed field. All data are then fluxed using 6dF observations of the standard stars Feige 110 and EG274. This fluxing is inevitably crude, in that the same fixed average spectral transfer function is assumed for each plate for all time. Differences in the transfer function between individual fibres are corrected for by the flat-fielding.

The resulting V and R spectra for each source are then spliced together, using the overlapping region to obtain their relative scaling. In order to avoid a dispersion discontinuity at the join in each spectrum, we also rescrunch the lower-dispersion R data on to an exact continuation of the V wavelength dispersion.

4.3 Spectral quality

Most spectra have no problems, in the sense that: (1) the S/N is reasonable given the magnitude of the source; (2) both V and R frames are available; and (3) there were no problems in the reduction. However, there are significant caveats of which all users should be aware.

(i) Many fields were observed in marginal conditions, and have reduced overall S/N as a result. Our philosophy has been to extract what good spectra we can from these fields, and recycle the rest for reobservation. A field was only reobserved in its entirety where the data was valueless.

(ii) Many fields were observed with three or occasionally even two guide fibres, with consequent lower and more variable S/N.

(iii) Some fibres have poor throughputs due to misalignment or poor glueing within the button, and variations of factors of 2 are normal.

(iv) Many fibres, throughout the duration of the survey, have suffered various damage in use, short of breakage. Very often, this has resulted in strong fringing in the spectral response of the fibre, due to an internal fracture acting as a Fabry –Perot filter. This did not often flat-field out completely.

(v) The CCD is in any case a thinned blue-sensitive chip; as a result, red data suffer increasing levels of fringing towards longer wavelengths, and this does not always flat-field out.

(vi) Fibre breakages during configuring, or between blue and red observations, or severe differences in acquisition, can lead to occasional missing or mis-spliced red or blue data.

(vii) Some fields have missing red data.

(viii) Though scattered light is not a major problem in general, data at the blue end of the spectra can be corrupted, because the actual counts are so low. In extreme cases, the spectra can become negative. The overall quality of the fluxing is untested, and should be treated with extreme caution.

(ix) All VPH data suffer from a faint but variable, spurious, spectral feature at wavelengths around 4440 Å (10-pixel region) in the V grating, and 6430 and 6470 Å (10-pixel regions) in the R. The reason, after extensive investigation, was determined to be a ghost caused by dispersed light reflected back off the grating and recollimated by the camera, being undispersed in first-order reflection mode by the VPH grating, and refocused on to the chip as a somewhat out-of-focus (10–20 pixel diameter), undispersed, image of the fibre, with an intensity 0.1–1 per cent of the summed dispersed light. Circumventing this problem requires tilting the fringes within the grating (so they are no longer parallel with the normal to the grating) by a degree or two, to throw the ghost image just off the chip.

4.4 Redshift measurement

Accurate redshift measurement is a fundamental component of both the *z*- and *υ*-surveys. We started with the semi-automated redshifting RUNZ software used for the 2dF Galaxy Redshift Survey (Colless et al. 2001b), kindly provided by Will Sutherland. Extensive modifications were made in order to accept 6dF data. The version used for 2dF determined quasi-independent estimators of the redshift from emission and absorption features; this improved the reliability of the redshift estimates, while reducing their accuracy. Since the line identification of the higher S/N and higher-dispersion 6dF spectra was usually not in doubt, we decided in general not to patch out emission features in determining cross-correlation redshifts; and in general the cross-correlation redshift was used in preference to the emission-line redshift.

Each automated redshift is checked visually to decide whether the software has made an accurate estimate or been misled by spurious spectral features. Such features are typically due to fibre interference patterns or poor sky subtraction and are difficult to identify through software, although easily recognizable to a human operator. The operator checks the automated redshift by comparing it to the original spectrum, the location of night-sky line features and the cross-correlation peak. In some cases, manual intervention in the form of refitting of spectral features or of the correlation peaks makes for a new redshift. In the majority of cases, however, the automated redshift value is accepted without change. The final redshift value is assigned a quality, Q, between 1 and 4 where $Q = 3$ or 4 for redshifts included in the final catalogue. $Q = 4$ represents a reliable redshift while $Q = 3$ is assigned to probable redshifts; $Q = 2$ is reserved for tentative redshift values and $Q = 1$ for spectra of no value. Fig. 4 shows a few examples of galaxy spectra across the range of redshift quality, for both emission- and absorption-line spectra.

The same visual assessment technique was employed for the 2dF Galaxy Redshift Survey and greatly increased the reliability of the final sample: repeat measurements on a set of ∼15 000 2dF spectra by two operators were discrepant in only 0.4 per cent of cases (Colless

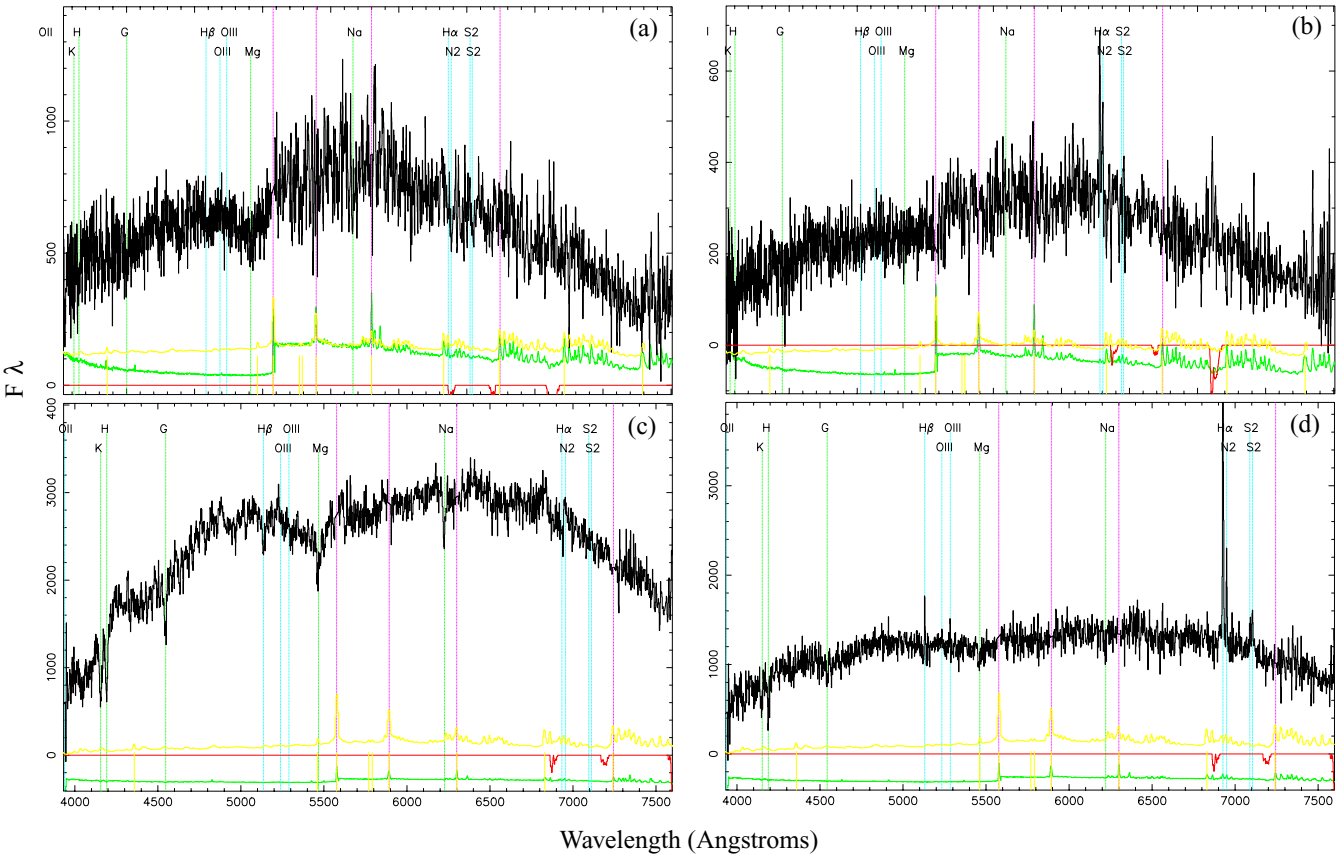

Figure 4. A colour version of this figure appears in the online version of the journal. Examples of galaxy spectra from the 6dFGS exhibiting a range of types and redshift quality Q: (a) $Q = 3$ absorption-line redshift at $z = 0.046\,01$. (b) $Q = 3$ emission-line redshift at $z = 0.033\,77$. (c) $Q = 4$ absorption-line redshift at $z = 0.056\,45$. (d) $Q = 4$ emission-line redshift at $z = 0.053\,44$. Also shown are the night-sky background emission (green spectrum), telluric transmission (red spectrum at $F_\lambda = 0$), and residual sky spectrum following sky-subtraction (yellow spectrum). Major absorption (green lines) and emission-line (cyan lines) features in the spectra have been labelled at the wavelengths corresponding to the redshift of each object. The wavelengths of strong night-sky features are also indicated (magenta lines).

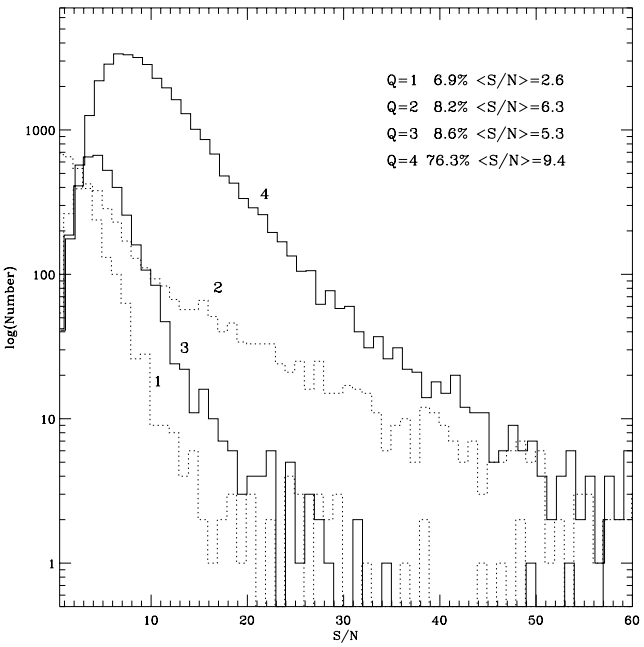

Figure 5. Distribution of signal-to-noise ratio for each class of redshift quality ($Q = 1$ to 4) for the 6dFGS.

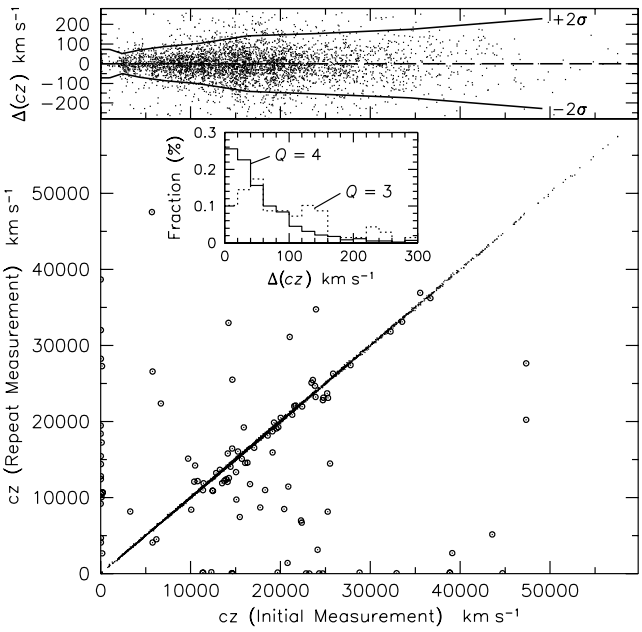

Figure 6. Comparison of initial and repeat 6dF redshift measurements for a sample of 4457 6dFGS galaxies. Redshift blunders (circled points) are those for which $|\Delta cz| > 370\,\mathrm{km\,s^{-1}}$ and represent 3.2 per cent of all points plotted. (Inset) Distribution of the $|\Delta cz|$ differences for the individual redshift quality $Q = 3$ (dotted line) and $Q = 4$ (solid line) samples. Each distribution has been normalized to the total sample size in each case (69 and 3574 sources, respectively). (Top panel) Distribution of redshift difference as a function of redshift, with a running $\pm 2\,\sigma$ boundary (solid lines).

et al. 2001b). Fig. 5 shows the relationship between redshift quality Q and mean signal-to-noise ratio of the spectra that yielded them. The vast majority (76 per cent) of the 6dFGS redshifts have $Q = 4$ from spectra with a median signal-to-noise ratio of 9.4 pixel^{-1}. For $Q = 3$ redshifts the median signal-to-noise ratio drops to 5.3 pixel^{-1}, indicating a minimum of range of redshift-yielding spectra. In both cases, note the long tail to higher signal-to-noise values. The median signal-to-noise ratio for $Q = 2$ redshifts (6.3 pixel^{-1}) is slightly higher than that for $Q = 3$ (5.3 pixel^{-1}). This is due to the significant number of Galactic sources such as stars and planetary nebulae, which produce high signal-to-noise spectra, but are assigned $Q = 2$ on account of their zero redshift. The Galactic sources will be reassigned to $Q = 3$ or 4 (as appropriate) on a later pass through the data set.

4.5 Redshift uncertainties and repeat measurements

There are 4457 galaxies for which a redshift with $Q \geqslant 3$ has been measured more than once. More often than not, repeat measurements are the result of fields that have been re-observed either because the first observation was incomplete or of poor quality; the other repeats occur when a galaxy lies in overlapping fields and is observed in each field. The rms scatter in the redshift differences $\Delta cz = cz(\mathrm{initial}) - cz(\mathrm{repeat})$ is $\sigma(\Delta cz) = 74\,\mathrm{km\,s^{-1}}$. We call repeat measurements that disagree by more than 5 $\sigma(\Delta cz) = 370\,\mathrm{km\,s^{-1}}$ 'blunders'. There are 143 blunders amongst the 4457 repeats – a pair-wise blunder fraction of 3.2 per cent. The rate at which blunders occur for a set of individual measurements is therefore 1.6 per cent, almost identical to that for the 2dFGRS (Colless et al. 2001b).

Fig. 6 shows a comparison of the repeat redshift measurements; the 143 blunders are circled. Many of the blunders lie close to the 1:1 line and are likely to be cases where one measurement has come from a low-S/N but usable spectrum, taken in poor conditions. Another group of blunders have $cz = 0\,\mathrm{km\,s^{-1}}$ for one measurement and are probably cases where the galaxy lies near a star

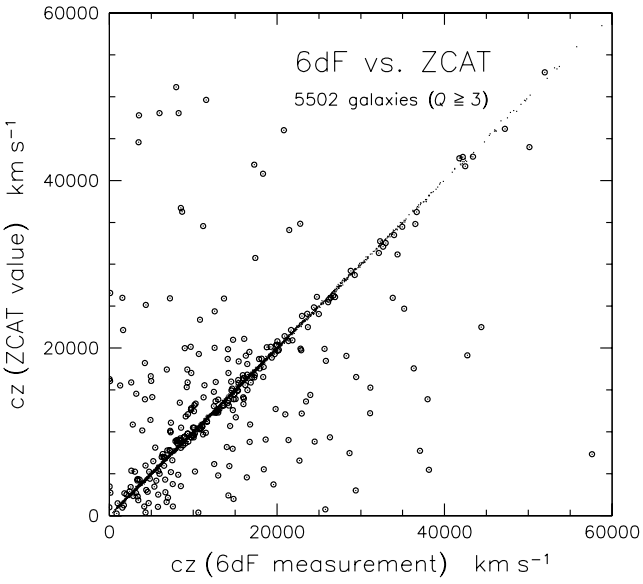

Figure 7. Comparison of 6dFGS redshifts for a set of galaxies with existing redshifts in the ZCAT catalogue. Redshift blunders (circled points) are those for which $|\Delta cz| > 370\,\mathrm{km\,s^{-1}}$ and represent 5.5 per cent of all points plotted.

which has dominated in one fibre position but not the other. The top panel of Fig. 6 shows the scatter in Δcz as a function of redshift. As expected, lower-redshift measurements exhibit a greater degree of repeatability than do those at higher redshift, reflecting the general trend towards fainter apparent magnitudes and lower-S/N

Table 4. Redshift uncertainties and blunder rates.

6dF repeat redshifts:	
Total repeat measurements ($Q \geqslant 3$):	4457
Number of blunders† ($Q \geqslant 3$):	143
6dFGS pair-wise blunder rate:	3.2 per cent
6dFGS single-measurement blunder rate:	1.6 per cent
$Q = 4$ redshift uncertainty (from 3574 sources)	46 km s^{-1}
$Q = 3$ redshift uncertainty (from 69 sources)	82 km s^{-1}
6dF versus ZCAT comparison:	
Number of unique comparison sources ($Q \geqslant 3$):	5502
Number of blunders[a] ($Q \geqslant 3$):	305
Pair-wise blunder rate:	5.5 per cent
Implied single-measurement	
Blunder rate for ZCAT:	4.0 per cent

[a]A blunder is a redshift difference $\Delta cz > 370\,\mathrm{km\,s^{-1}}$, equivalent to five times the rms error in the full sample of 6dF-to-6dF redshift differences.

spectra. Table 4 summarizes the fractional blunder rates for each sample.

The non-blunder sample contains 3574 (83 per cent) pairs with redshift qualities (Q_1, Q_2) = (4, 4), 671 (15 per cent) (3, 4)-pairs and 69 (2 per cent) (3, 3)-pairs. The rms scatter in the (4, 4)-sample is 65 km s^{-1}, implying a redshift uncertainty for a single $Q = 4$ measurement of $\Delta cz(4) = 46\,\mathrm{km\,s^{-1}}$. Similarly, the rms scatter in the much smaller (3, 3)-sample is 116 km s^{-1} and so $\Delta cz(3) = 82\,\mathrm{km\,s^{-1}}$. These single-measurement values are consistent with the scatter in the (3, 4)-pairs, $\Delta cz(3, 4) = 95\,\mathrm{km\,s^{-1}}$, which equals $[\Delta cz^2(4) + \Delta cz^2(3)]^{1/2}$. The inset in Fig. 6 shows the $|\Delta cz|$ distributions for the $Q = 3$ and $Q = 4$ non-blunder samples, normalized to the total number in each sample.

We have also made an external comparison of 6dF-measured redshifts with those of the ZCAT catalogue (Huchra et al. 1999). In Fig. 7 we apply the same $|\Delta cz| > 370\,\mathrm{km\,s^{-1}}$ blunder cut to the 5502 galaxies holding both $Q \geqslant 3$ 6dF and ZCAT redshifts. There are 305 blunders, yielding the higher pair-wise blunder rate of 5.5 per cent. We know from the internal comparison above that the 6dF single-measurement blunder fraction is 1.6 per cent, implying that the blunder rate for individual ZCAT measurements is around 4 per cent. This is understandable given that ZCAT is a heterogeneous compilation of redshifts from a range of source materials of varying quality. Colless et al. (2001b) similarly find that the scatter between ZCAT and 2dFGRS redshifts is significantly higher than in comparisons between 2dFGRS and redshifts from the CfA2, SAPM, PSCz and LCRS surveys. They estimate that the single-measurement blunder rate of ZCAT redshifts is 5.0 per cent.

5 FIRST DATA RELEASE

5.1 Statistics and plots

Between 2002 January and 2003 July the 6dF Galaxy Survey Data Base compiled 52 048 spectra from which 46 474 unique galaxy redshifts were derived. The numbers of spectra with redshift quality $Q \geqslant 3$ were 43 945 for the full set and 39 649 for the unique redshifts. Of the 174 442 total galaxies in the target sample, 28 014 had existing literature redshifts: 19 570 from the ZCAT compilation (Huchra et al. 1999) and 8444 from the 2dF Galaxy Redshift Survey (Colless et al. 2001b). Of the 113 988 K-selected sources, there are 32 156 6dF-measured redshifts of redshift quality $Q \geqslant 3$, plus a further 21 151 existing literature redshifts. Table 5 summarizes these values for the individual subsamples as they appear in the 6dFGS Data Base.

Data from 524 fields have contributed to the first data release. As shown in Fig. 8 (top), the majority of these occupy the central declination strip $-42^\circ < \delta < -23^\circ$. Overall there are 1564 on the sky: 547 in the equatorial strip, 595 in the central strip, and 422 in the

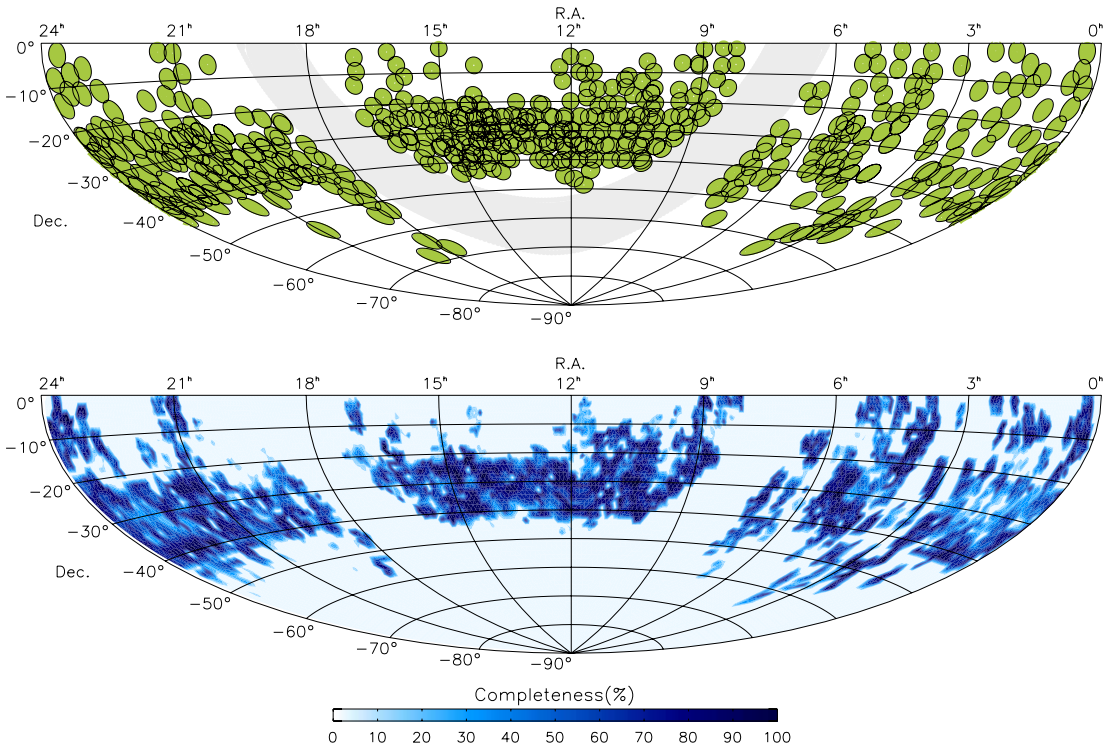

Figure 8. A colour version of this figure appears in the online version of the journal. Top: location of the observed fields (green discs) contributing redshifts to the First Data Release. Bottom: redshift completeness on the sky, combining the 6dF First Data Release redshifts with the literature sources.

Table 5. Status of the 6dFGS target samples, as listed in the data base.

ID	Survey	Total	$cz \leqslant 600$	$cz > 600$	6df z	lit z	6df >600	Q34	Q1	Q2	Q3	Q4	no z
1	2MASS $K < 12.75$	113988	1750	53051	33650	21151	32983	32156	1312	1494	2708	29448	59187
3	2MASS $H < 13.05$	3282	18	853	526	345	512	492	33	34	58	434	2411
4	2MASS $J < 13.75$	2008	17	552	333	236	319	304	14	29	28	276	1439
5	DENIS $J < 14.00$	1505	11	259	124	146	117	111	26	13	27	84	1235
6	DENIS $I < 14.85$	2017	96	191	150	137	63	63	18	87	10	53	1730
7	SuperCOSMOS $r_F < 15.6$	9199	137	3310	1539	1908	1439	1407	46	132	104	1303	5752
8	SuperCOSMOS $b_J < 16.75$	9749	35	3718	1973	1780	1961	1900	76	73	173	1727	5996
78	Durham/UKST extension	466	2	73	10	65	8	8	1	2	6	2	391
90	Shapley supercluster	939	9	323	282	50	273	250	22	32	48	202	607
113	*ROSAT* All-Sky Survey	2913	99	535	395	239	300	223	231	172	53	170	2279
116	2MASS red AGN Survey	2132	9	252	129	132	121	81	106	48	45	36	1871
119	HIPASS ($>4\,\sigma$)	821	8	268	135	141	130	121	11	14	29	92	545
125	SUMSS/NVSS radio sources	6843	321	709	654	376	347	322	89	332	51	271	5813
126	IRAS FSC ($6\,\sigma$)	10707	258	2872	1360	1770	1218	1105	303	255	198	907	7577
129	Hamburg-ESO Survey QSOs	3539	73	197	220	50	150	56	204	164	19	37	3269
130	NRAO-VLA Sky Surv. QSOs	4334	342	146	483	5	142	62	303	421	42	20	3846
	Total	174442	3185	67309	41963	28531	40083	38661	2795	3302	3599	35062	103948

Column headings:
$cz \leqslant 600$ – object has a redshift (either 6dF-measured with quality >1 or from the literature) less than or equal to 600 km s^{-1}.
$cz > 600$ – object has a redshift (either 6dF-measured with quality >1 or from the literature) greater than 600 km s^{-1}.
6df z – total number of 6dF-measured redshifts with quality $Q > 1$.
lit z – total number of literature redshifts.
6df >600 – number of 6dF-measured redshifts greater than 600 km s^{-1} with quality $Q > 1$.
Q34 – total number of (6dF-measured) sources with redshift quality $Q = 3$ or 4.
Q1, Q2, Q3, Q4 – total number of sources with redshift quality $Q = 1$, $Q = 2$, $Q = 3$, $Q = 4$.
no z – number of sources in the data base with neither a 6dF (quality $Q > 1$) nor literature redshift.

polar region. Fig. 8 (bottom) shows the corresponding distribution of redshift completeness on the sky for the K-band sample. The *redshift completeness*, R, is that fraction of galaxies in the parent catalogue of 174 442 with acceptable ($Q \geqslant 3$) redshifts in a given area of sky, from whatever source,

$$R = \frac{N_z(\boldsymbol{\theta})}{N_p(\boldsymbol{\theta})} = \frac{N_{lit}(\boldsymbol{\theta}) + N_{6dF}(\boldsymbol{\theta})}{N_{lit}(\boldsymbol{\theta}) + N_{6dF}(\boldsymbol{\theta}) + N_{Gal}(\boldsymbol{\theta}) + N_f(\boldsymbol{\theta}) + N_r(\boldsymbol{\theta})}. \quad (2)$$

Here, $N_p(\boldsymbol{\theta})$ is the number of galaxies from the parent catalogue (per unit sky area) at the location $\boldsymbol{\theta}$, and $N_z(\boldsymbol{\theta})$ is the number with redshifts, either from 6dF ($N_{6dF}(\boldsymbol{\theta})$) or the literature ($N_{lit}(\boldsymbol{\theta})$). Sources in the parent catalogue that have been redshifted and excluded are either stars, planetary nebulae/ISM features (both assigned $Q = 2$), or failed spectra ($Q = 1$). In equation (2) their numbers are denoted by $N_{Gal}(\boldsymbol{\theta})$ and $N_f(\boldsymbol{\theta})$. The remaining sources are those yet to be observed, $N_r(\boldsymbol{\theta})$. Of the first ~41 000 sources observed with 6dF, around 3 per cent were stars, 1 per cent were other Galactic sources, and 11 per cent failed to yield a redshift.

The *field completeness* is the ratio of acceptable redshifts in a given field to initial sources, and hence is only relevant to targets observed with 6dF. It also excludes Galactic features like stars and ISM. Fig. 9 shows the distribution of field completeness from the first 524 fields and its cumulate. This demonstrates that the redshift success rate of 6dF is good, with both the median and mean completeness around 90 per cent.

Observe the large difference between the high *field* completeness values of Fig. 9 and the lower *redshift* completeness in Fig. 8 (bottom). This is due to the high degree of overlap in the 6dFGS field allocation. The large variance in the density of targets has meant that most parts of the sky need to be tiled two or more times

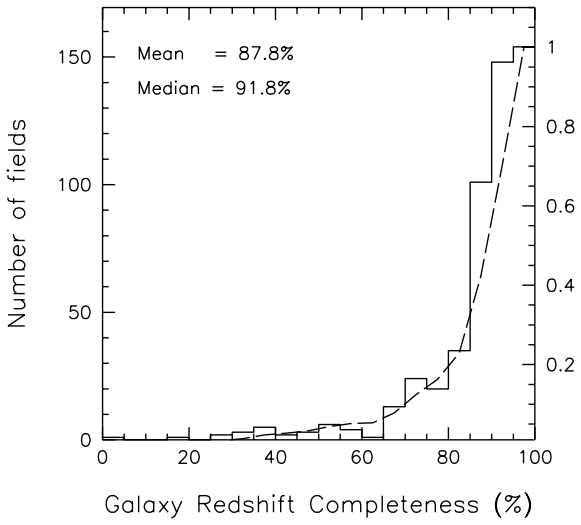

Figure 9. Galaxy redshift completeness by field, where completeness is the number of 6dF redshifts over the total 6dF redshifts and failures. The dashed line indicates the cumulative fraction according to the right-hand axis.

over. This is not at all obvious in Fig. 8 (top) which superimposes all fields, giving the impression of a single layer of tiles. While much of the central strip contains observed and redshifted fields, it also contains other fields in this same region, as yet unobserved.

In Fig. 10 we show the distribution of 6dFGS redshifts compared to those of other surveys. The 6dFGS redshift distribution exhibits the classic shape for magnitude-limited surveys of this kind. The median survey redshift, $\bar{z} = 0.054$, doubles that of the earlier PSCz

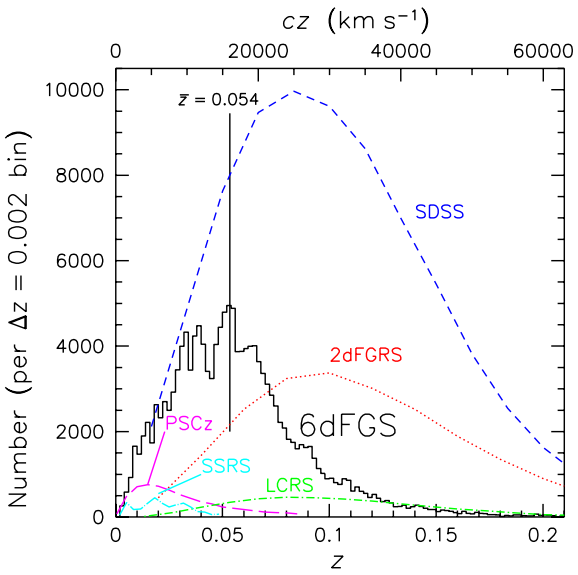

Figure 10. A colour version of this figure appears in the online version of the journal. Number –redshift distribution for the 6dF Galaxy Survey, comprising First Data Release galaxies with redshift quality $Q \geqslant 3$ and $cz > 600\,\mathrm{km\,s^{-1}}$. The mean redshift for the survey ($\bar{z} = 0.054$) is indicated with a vertical solid line. Also shown are the equivalent distributions for the SDSS (short dashed line, blue), 2dFGRS (dotted line, red), PSCz (long dashed line, magenta), SSRS (dot-dash line, cyan) and LCRS (dot-dash line, green) surveys listed in Table 1. All curves have been normalized to yield the total sample sizes given in Table 1.

and SSRS surveys, but is less than half that of 2dFGRS and SDSS. In terms of sample size, the 6dFGS and SDSS will be comparable over the nearest volumes ($z \leqslant 0.05$) when complete, and exceed all other redshift surveys (including 2dFGRS) in this regime. Clearly the 6dFGS provides coverage of the local Universe at an unprecedented level of detail.

Fig. 11 shows the radial distribution of galaxies across the southern sky, projected across the full range of southerly declinations ($\delta = 0$ to $-90°$). Projecting in this way has the drawback of taking truly separate 3D space structures and blending them on the 2D page. Fig. 12 shows the same data plotted in $\Delta\delta = 10°$ declination slices and a magnified view of the lowest-redshift galaxies within $-40° < \delta < -30°$.

Variations in galaxy density apparent in Figs 11 and 12 are due the incomplete coverage of observed fields and the projection of the Galactic plane. No 6dFGS galaxies lie within galactic latitude $|b| \leqslant 10°$. The 6dFGS is also clumpier than optically selected redshift surveys such as 2dFGRS and SDSS. This is because the near-infrared selection is biased towards early-type galaxies, which cluster more strongly than spirals.

The 6dFGS provides the largest sample of near-infrared selected galaxies to determine the fraction of mass in the present-day Universe existing in the form of stars. To this end, Jones, Colless & Saunders (in preparation) are deriving the *J*-, *H*- and *K*-band luminosity functions from the first 82 000 redshifts of the 6dF Galaxy Survey, combining data from both before and after the First Data Release. Using the near-infrared luminosity functions and stellar population synthesis models, the galaxy stellar-mass function for the local Universe can be estimated. When this is integrated over the full range of galaxy masses, the total mass of the present-day Universe in stars can be expressed in units of the critical density.

5.2 6dFGS online data base

Data from the 6dF Galaxy Survey are publicly accessible through an online data base at http://www-wfau.roe.ac.uk/6dFGS/, and maintained by the Wide Field Astronomy Unit of the Institute for Astronomy, University of Edinburgh. An early data release of around 17 000 redshifts was made in 2002 December, along with the opening of the Web site and tools for catalogue access. This paper marks the First Data Release of 52 048 total redshifts measured between 2002 January and 2003 July. The design of the data base is similar to that used for the 2dF Galaxy Redshift Survey in that parametrized data are stored in a relational data base. Each TARGET object is also represented by a multi-extension FITS file which holds thumbnail images of the object and the spectra. The data base is accessed/queried using Structured Query Language (SQL). A combined 6dF-literature redshift catalogue is provided in a separate single master catalogue.

The 6dFGS data base is housed under Microsoft's relational data base software, SQL *Server 2000*. The data are organized in several tables (Table 6). The master target list used to configure 6dFGS observations is represented by the TARGET table. Spectral observations are stored in the SPECTRA table. The input catalogues that were merged to make up the master target list are also held in individual tables (TWOMASS, SUPERCOS etc.). The TARGET table forms the hub of the data base. Every table is interlinked via the parameters TARGETID and TARGETNAME. These parameters are unique in the master TARGET table but are not necessarily unique in the other tables (e.g. SPECTRA), as objects can and have been observed more than once. The SPECTRA table holds all the observational and redshift related data. Parameters are recorded for both the V and R frames (with a lot of the values being the same for both frames), and redshift information is derived from the combined VR frame. The TWOMASS table contains the *K*, *J* and *H*-selected samples originating from the 2MASS extended source catalogue. The *K*-selected sample represents the primary 6dFGS input catalogue. Table 6 lists the programme details for the other contributing samples.

Initially every FITS file, representing each target (TARGETNAME.FITS), holds thumbnail images of the target. As data are ingested into the data base the reduced spectra are stored as additional FITS image extensions. Table 7 summarizes the content within each FITS extension. The first five extensions contain the thumbnail images and each have a built-in World Coordinate System (WCS). The optical *B* and *R* images come from SuperCOSMOS scans of blue b_J and red r_F survey plates. The 2MASS *J*, *H* and *K* images were extracted from data cubes supplied by IPAC. Note that although some objects in TARGET do not have 2MASS images, the corresponding extensions still exist in the FITS file but contain small placeholder images. The remaining extensions contain the spectra. Each 6dFGS observation will usually result in a further three extensions, the V grating spectrum, the R spectrum and the combined/spliced VR spectrum.

The V and R extensions are images with three rows. The first row is the observed reduced SPECTRUM, the second row is the associated variance and the third row stores the SKY spectrum as recorded for each data frame. Wavelength information is provided in the header keywords CRVAL1, CDELT1 and CRPIX1, such that

$$\text{wavelength (Å)} = \text{CRVAL1} - (\text{CRPIX1} - \text{pixel number}) \times \text{CDELT1}. \quad (3)$$

Additional WCS keywords are also included to ensure the wavelength information is displayed correctly when using image browsers such as GAIA or SAOimage DS9 in Starlink.

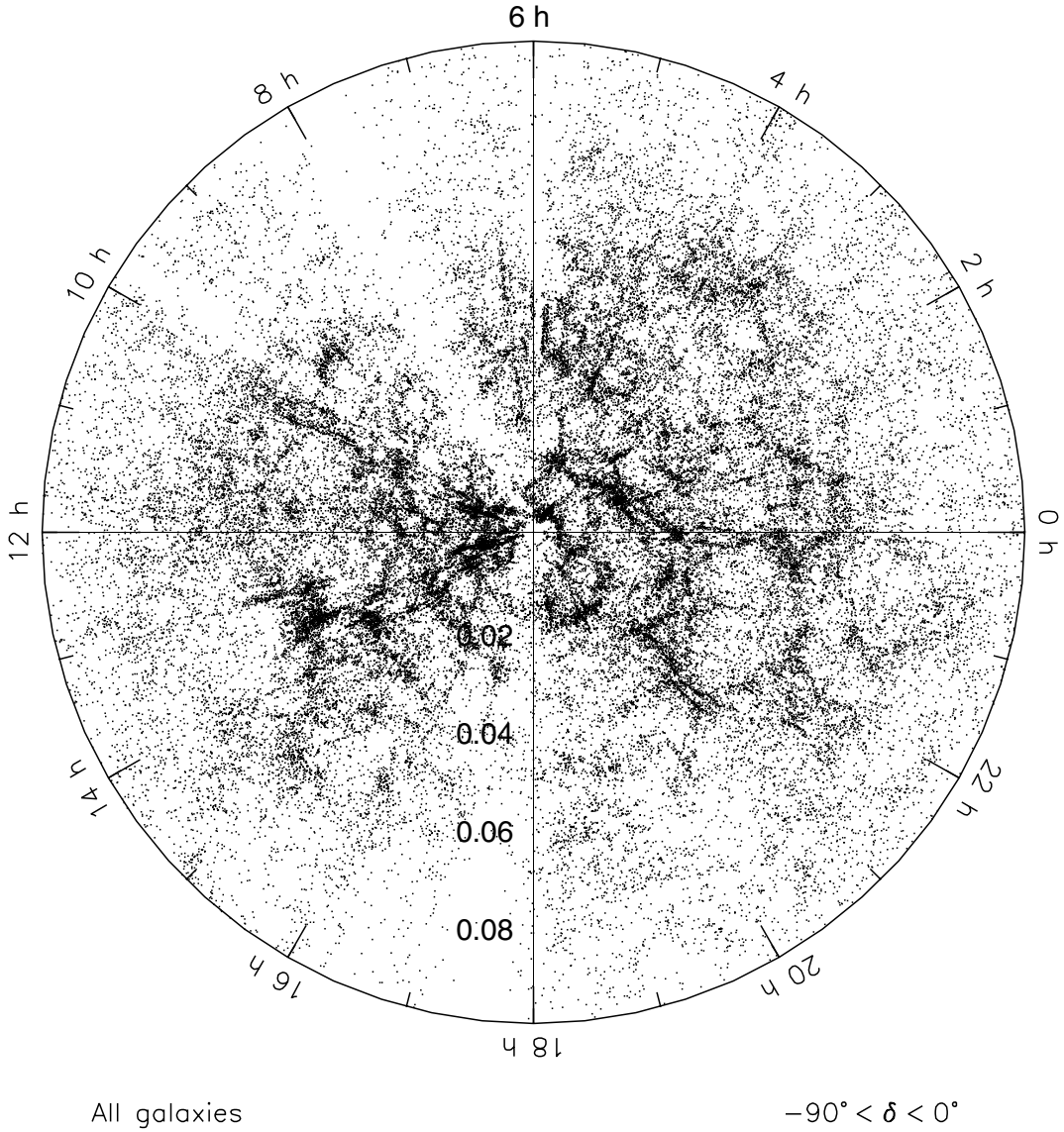

Figure 11. Spatial redshift distribution combining the 6dF and literature redshifts. The redshift slice projects through all southerly declinations, $\delta < 0^\circ$. The sparse sampling around 8 and 17 hr is due to non-coverage in the Galactic plane. Variations elsewhere in the sky are due to different sky regions having different observational completenesses at the time of this First Data Release.

The VR extension also has an additional fourth row that represents the WAVELENGTH axis, which has a continuous dispersion, achieved through the continuation of the V dispersion into the R half from rescrunching.

Access to the data base is through two different Hypertext Markup Language (HTML) entry forms. Both parse the user input and submit an SQL request to the data base. For users unfamiliar with SQL, the menu driven form provides guidance in constructing a query. The SQL query box form allows users more comfortable with SQL access to the full range of SQL commands and syntax. Both forms allow the user to select different types of output (HTML, comma separated value (CSV) or a TAR save-set of FITS files).

There are online examples of different queries using either the menu or SQL form at http://www-wfau.roe.ac.uk/6dFGS/examples.html. More information about the data base is available directly from the 6dFGS data base Web site.

6 CONCLUSIONS

The 6dF Galaxy Redshift Survey (6dFGS) is designed to measure redshifts for approximately 150 000 galaxies and the peculiar velocities of 15 000. The survey uses the 6dF multifibre spectrograph on the United Kingdom Schmidt Telescope, which is capable of observing up to 150 objects simultaneously over a 5.°7-diameter field of view. The 2MASS Extended Source Catalog (Jarrett et al. 2000) is the primary source from which targets have been selected. The primary sample has been selected with $K_{\rm tot} \leqslant 12.75$, where $K_{\rm tot}$ denotes the total K-band magnitude as derived from the isophotal 2MASS K photometry. Additional galaxies have been selected to complete the target list down to $(H, J, r_{\rm F}, b_{\rm J}) = (13.05, 13.75, 15.6, 16.75)$. Thirteen miscellaneous surveys complete the total target list.

The survey covers the entire southern sky (declination $\delta < 0^\circ$), save for the regions within $|b| \leqslant 10^\circ$ of the Galactic plane. This

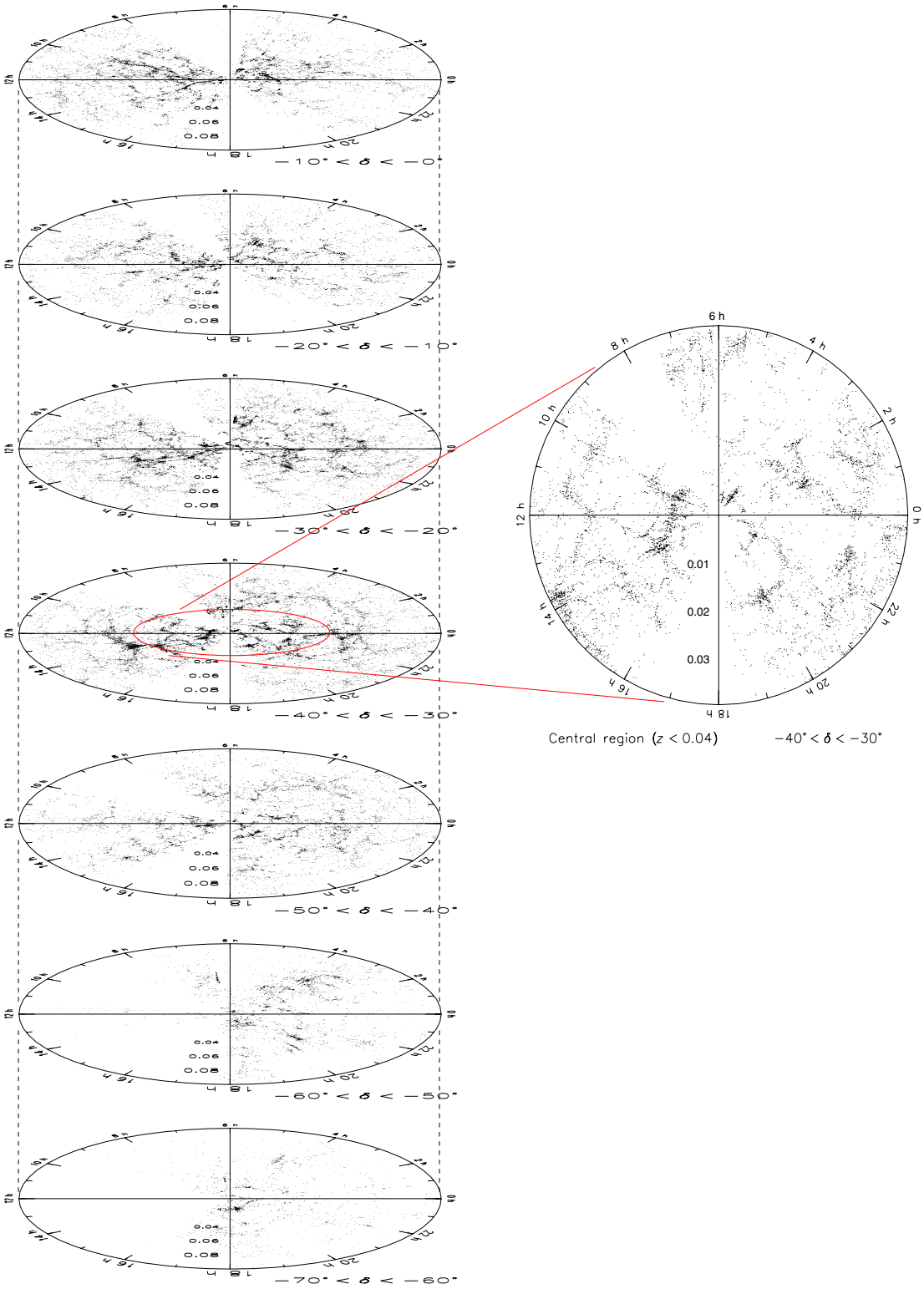

Figure 12. Spatial redshift distribution divided into discs, each spanning a 10° range in declination. The inset shows an expanded view of the central region of the $-40^\circ < \delta < -30^\circ$ slice.

area has been tiled with around 1500 fields that effectively cover the southern sky twice over. An adaptive tiling algorithm has been used to provide a uniform sampling rate of 94 per cent. In total the survey covers some 17 046 deg^2 and has a median depth of $\bar{z} = 0.05$. There are three stages to the observations, which initially target the declination strip $-42^\circ < \delta < -23^\circ$, followed by the equatorial region $-23^\circ < \delta < 0^\circ$, and conclude around the pole ($\delta < -42^\circ$).

Spectra are obtained through separate V and R gratings and later spliced to produce combined spectra spanning 4000–8400 Å. The spectra have 5–6 Å FWHM resolution in V and 9–12 Å resolution in

Table 6. Tables of data in the 6dFGS data base.

Table name	Description	Programme ID numbers
TARGET	the master target list	PROGID
SPECTRA	redshifts and observational data	–
TWOMASS	2MASS input catalogue K, H, and J	1, 3, 4
SUPERCOS	SuperCOSMOS bright galaxies b_J and r_F	7, 8
FSC	sources from the IRAS FAINT Source Catalogue	126
RASS	candidate AGN from the *ROSAT* All-Sky Survey	113
HIPASS	sources from the HIPASS HI survey	119
DURUKST	extension to Durham/UKST galaxy survey	78
SHAPLEY	galaxies from the Shapley supercluster	90
DENISI	galaxies from DENIS $I < 14.85$	6
DENISJ	galaxies from DENIS $J < 13.85$	5
AGN2MASS	candidate AGN from the 2MASS red AGN survey	116
HES	candidate QSOs from the Hamburg/ESO Survey	129
NVSS	candidate QSOs from NVSS	130
SUMSS	radio source IDs from SUMSS and NVSS	125

Table 7. Contents of each extension in the data base FITS files.

FITS Extension	Contents
1st	SuperCOSMOS b_J image (1×1 arcmin^2)
2nd	SuperCOSMOS r_F image (1×1 arcmin^2)
3rd	2MASS J image (variable size)
4th	2MASS H image (variable size)
5th	2MASS K image (variable size)
6th	V-spectrum extension
7th	R-spectrum extension
8th	combined VR-spectrum extension
nth	additional V, R, and VR data

R. Software is used to estimate redshifts from both cross-correlation with template absorption-line spectra, and linear fits to the positions of strong emission lines. Each of these automatic redshift estimates is checked visually and assigned a quality Q on a scale of 1 to 4, where $Q \geqslant 3$ covers the range of reliable redshift measurements. The median signal-to-noise ratio is 9.4 pixel^{-1} for redshifts with quality $Q = 4$, and 5.3 pixel^{-1} for $Q = 3$ redshifts.

The data in this paper constitute the First Data Release of 52 048 observed spectra and the 46 474 unique extragalactic redshifts from this set. The rates of contamination by Galactic and failed spectra are 4 per cent and 11 per cent, respectively. Data from the 6dF Galaxy Survey are publicly available through an online data base at http://www-wfau.roe.ac.uk/6dFGS/, searchable through either SQL query commands or an online WWW form. The main survey Web site can be found at http://www.mso.anu.edu.au/6dFGS.

ACKNOWLEDGMENTS

We acknowledge the efforts of the staff of the Anglo-Australian Observatory, who have undertaken the observations and developed the 6dF instrument. We are grateful to P. Lah for his help in creating Fig. 11. We are also grateful to an anonymous referee for several suggestions which enhanced the content and presentation of the paper. DHJ is supported as a Research Associate by Australian Research Council Discovery –Projects Grant (DP-0208876), administered by the Australian National University.

TJ and JH acknowledge the support of NASA. They are grateful to the other members of the 2MASS extragalactic team, M. Skrutskie, R. Cutri, T. Chester and S. Schneider for help in producing the major input catalogue for the 6dFGRS. They also thank NASA, the NSF, the USAF and USN and the State of Massachussetts for the support of the 2MASS project and NASA for the support of the 6dF observational facility.

The DENIS project has been partly funded by the SCIENCE and the HCM plans of the European Commission under grants CT920791 and CT940627. It is supported by INSU, MEN and CNRS in France, by the State of Baden-Warttemberg in Germany, by DGICYT in Spain, by CNR in Italy, by FFwFBWF in Austria, by FAPESP in Brazil, by OTKA grants F-4239 and F-013990 in Hungary, and by the ESO C & EE grant A-04-046.

REFERENCES

Bell E. F., McIntosh D. H., Katz N., Weinberg M. D., 2003, ApJS, 149, 289
Blanton M. R. et al., 2001, AJ, 121, 235, 8
Blanton M. R., Lin H., Lupton R. H., Maley F. M., Young N., Zehavi I., Loveday J., 2003, AJ, 125, 2276
Branchini E. et al., 1999, MNRAS, 308, 18
Burkey D., 2004, PhD thesis, Univ. Edinburgh
Burkey D., Taylor A. 2004, MNRAS, 347, 255
Campbell L. A., Saunders W., Colless M., 2004, MNRAS, 350, 1467
Cole S. et al., (2dFGRS team), 2001, MNRAS, 326, 255
Colless M. M., Saglia R. P., Burstein D., Davies R. L., McMahan R. K., Wegner G., 2001a, MNRAS, 321, 277
Colless M. M. et al., (2dFGRS team), 2001b, MNRAS, 328, 1039
Cross N. et al., (2dFGRS team), 2001, MNRAS, 324, 825
da Costa L. N. et al., 1998, AJ, 116, 1
da Costa L. N., Bernardi M., Alonso M. V., Wegner G., Willmer C. N. A., Pellegrini P. S., Maia M. A. G., Zaroubi S., 2000, ApJ, 537, L81
De Propris R. et al., (2dFGRS team), 2002, MNRAS, 329, 87
Djorgovski S., Davis M., 1987, ApJ, 313, 59
Dressler A., Lynden-Bell D., Burstein D., Davies R. L., Faber S. M., Terlevich R., Wegner G., 1987, ApJ, 313, 42
Efstathiou G. et al., (2dFGRS team), 2002, MNRAS, 330, 29
Folkes S. et al., (2dFGRS team), 1999, MNRAS, 308, 459
Giovanelli R., Haynes M. P., Salzer J. J., Wegner G., da Costa L. N., Freudling W., 1998, AJ, 116, 2632
Goto T. et al., 2003, PASJ, 55, 739
Hambly N. C. et al., 2001, MNRAS, 326, 1279
Hawkins E. et al., (2dFGRS team), 2003, MNRAS, 346, 78

Hoeg E. et al., 2000, A&A, 355, L27
Huchra J., Vogeley M. S., Geller M. J., 1999, ApJS, 121, 287
Hudson M. J., Smith R. J., Lucey J. R., Schlegel D. J., Davies R. L., 1999, ApJ, 512, L79
Jarrett T. H., Chester T., Cutri R., Schneider S., Rosenberg J., Huchra J. P., Mader J., 2000, AJ, 120, 298
Kochanek C. S. et al., 2001, ApJ, 560, 566
Lahav O. et al., (2dFGRS team), 2002, MNRAS, 333, 961
Lauer T. R., Postman M., 1994, ApJ, 425, 418
Lewis I. J. et al., 2002, MNRAS, 333, 279
Loveday J., Peterson B. A., Efstathiou G., Maddox S. J., 1992, ApJ, 390, 338
Lynden-Bell D., Faber S. M., Burstein D., Davies R. L., Dressler A., Terlevich R. J., Wegner G., 1988, ApJ, 326, 19
Madgwick D. S. et al., (2dFGRS team), 2002, MNRAS, 333, 133
Metropolis N., Rosenbluth A. W., Rosenbluth M. N., Teller A. H., Teller E., 1953, J. Chem. Phys., 21
Norberg P. et al. (2dFGRS team), 2002, MNRAS, 336, 907
Parker Q. A., Watson F. G., Miziarski S., 1998, in Arribas S., Mediavilla E., Watson F., eds, ASP Conf. Ser. Vol. 152, Fiber Optics in Astronomy III. Astron. Soc. Pac., San Francisco, p. 80
Parker Q. A., Watson F. G., 1995, in Barden S., ed., Fiber Optics in Astronomical Applications. Proc SPIE v2476, p. 34
Peacock J. A. et al., (2dFGRS team), 2001, Nat, 410, 169
Percival W. J. et al., (2dFGRS team), 2001, MNRAS, 327, 1297
Saunders W. et al., 2000, MNRAS, 317, 55
Saunders W. et al., 2001, AAO Newsletter, 97, 14
Scaramella R., Baiesi-Pillastrini G., Chincarini G., Vettolani G., Zamorani G., 1989, Nat, 338, 562
Szalay A. et al., 2003, ApJ, 591, 1
Verde L. et al., (2dFGRS team), 2002, MNRAS, 335, 432
Watson F. G., Parker Q. A., Bogatu G., Farrell T. J., Hingley B. E., Miziarski S., 2000, in Iye M., Moorwood A. F., eds, Proc. SPIE Vol. 4008, Optical and IR Telescope Instrumentation and Detectors. SPIE, Bellingham, WA, p. 123
Wegner G. A., Colless M., Saglia R. P., McMahan R. K., Davies R. L., Burstein D., Baggley G., 1999, MNRAS, 305, 259
York D. G. et al. (SDSS team), 2000, AJ, 120, 1579
Zehavi I. et al., (SDSS team), 2002, ApJ, 571, 172

This paper has been typeset from a TEX/LATEX file prepared by the author.